Available online at www.sciencedirect.com
ScienceDirect
Trans. Nonferrous Met. Soc. China 29(2019) 2506−2513
Transactions of Nonferrous Metals Society of China
www.tnmsc.cn

Effect of Li content on microstructure and mechanical property of Mg−*x*Li−3(Al−Si) alloys

Cheng ZHANG[1,2], Liang WU[1,2], Zi-long ZHAO[3], Zhi-hui XIE[4], Guang-sheng HUANG[1,2,5], Lei LIU[1,2], Bin JIANG[1,2,5], Andrej ATRENS[6], Fu-sheng PAN[1,2,5]

1. State Key Laboratory of Mechanical Transmission, College of Materials Science and Engineering, Chongqing University, Chongqing 400044, China;
2. National Engineering Research Center for Magnesium Alloys, Chongqing University, Chongqing 400044, China;
3. College of Civil Engineering, Chongqing University, Chongqing 400045, China;
4. Synthesis and Pollution Control Key Laboratory of Sichuan Province, College of Chemistry and Chemical Engineering, China West Normal University, Nanchong 637002, China;
5. Chongqing Research Center for Advanced Materials, Chongqing Academy of Science and Technology, Chongqing 401123, China;
6. School of Mechanical and Mining Engineering, The University of Queensland, Brisbane Qld 4072, Australia

Received 12 March 2019; accepted 16 October 2019

Abstract: Mg−4Li−3(Al−Si), Mg−8Li−3(Al−Si) and Mg−12Li−3(Al−Si) alloys based on the α-Mg, α-Mg+β-Li, β-Li phases, respectively, were produced to investigate the effect of alloying with Al−Si eutectic on the microstructure and mechanical properties of the three alloys. Alloying with the Al−Si eutectic of Mg−*x*Li (*x*=4, 8 and 12 wt.%) alloys caused the formation of different types of Al−Li precipitates: Al_3Li, AlLi and Li_3Al_2, respectively. Also, considerable quantities of Mg_2Si phase particles were found in the three alloys. The results of tensile tests showed that the Mg−4Li−3(Al−Si) alloy exhibited the highest ultimate tensile strength (UTS) of 249 MPa but the lowest elongation of 6.3%. The Mg−12Li−3(Al−Si) alloy had the highest elongation of 26% but the lowest UTS of 173 MPa. The different mechanical properties were attributed to the different crystal structures of the three alloys and the precipitate with different type, morphology and distribution.

Key words: Mg−Li alloy; Al−Si eutectic; second phase; tensile strength; elongation

1 Introduction

Magnesium (Mg) alloys are the lightest metallic material used for structural applications such as transportation and aerospace, owing to their low density, high specific strength, and high damping capacity [1−6]. However, Mg alloys have poor deformability and poor ductility at room temperature because of their hexagonal closed packed (HCP) crystal structure, and consequently their limited number of slip systems. Fortunately, alloying with Li has a great potential to produce Mg−Li alloys with good ductility due to the change of the HCP crystal structure to a body-center cubic (BCC) crystal structure [7,8]. Furthermore, alloying with Li can further reduce the density of Mg alloys. Mg−*x*Li alloys exhibit three different kinds of crystal structure with increasing Li content. Mg−*x*Li alloys have a HCP crystal structure and an α-Mg-based microstructure for x<5.7 wt.%, a combination of HCP+BCC crystal structures and a combination of α-Mg and β-Li in their microstructure for 5.7 wt.%<x<10.3 wt.%, and a BCC crystal structure and a microstructure composed of β-Li for x>10.3 wt.% [9,10].

However, Mg−Li alloys typically possess low strength despite their good ductility [11,12]. Alloying with Al is a common effective approach to improve the

Foundation item: Projects (51971040, 51701029, 51671041, 51531002) supported by the National Natural Science Foundation of China; Project (2016YFB0301100) supported by the National Key Research and Development Program of China; Projects (2018T110943, 2017M620410) supported by the China Postdoctoral Science Foundation; Project (Xm2017010) supported by the the Chongqing Postdoctoral Scientific Research Foundation, China; Project (2018CDGFCL005) supported by the Fundamental Research Funds for the Central Universities, China
Corresponding author: Liang WU; E-mail: wuliang@cqu.edu.cn
DOI: 10.1016/S1003-6326(19)65158-7

strength of Mg−Li alloys [13,14], but the stability of these alloys is relatively poor due to metastability of the Al−Li compounds [15,16]. Alloying with Si can improve the strength and stability of the Mg−Li alloy [17,18], but these alloys can be difficult to produce because of the high melting temperature of the Mg−Si master alloys. A practical production method is to first produce an Al−Si eutectic alloy, and to add the Al−Si eutectic alloy to the Mg−Li alloy. SHI et al [17] studied the effect of alloying with Al and the Al−Si eutectic alloy on the microstructure and the mechanical properties of Mg−8Li alloys. The Mg−8Li−6(Al−Si) alloy had a tensile strength higher than the Mg−8Li, Mg−8Li−3Al and Mg−8Li−3(Al−Si) alloys, which was attributed to the refinement of the microstructure and the precipitation strengthening by the Mg_2Si, $MgLi_2Al$ and AlLi phase particles. Similarly, ZHAO et al [18] investigated the influence of alloying with Al and the Al−Si eutectic alloy on the microstructure and the mechanical properties of Mg−4Li alloys. The Mg−4Li−6(Al−Si) alloy had a tensile strength higher than the Mg−4Li, Mg−4Li−3Al and Mg−4Li−3(Al−Si) alloys, which was also attributed to the precipitation strengthening imparted by the Al_3Li(Mg) and Mg_2Si phase particles.

However, the effects of alloying with the Al−Si eutectic alloy on microstructure and mechanical properties of Mg−Li alloys with three different crystal structures (HCP structure, HCP+BCC structure, BCC structure) have not been systematically studied. Moreover, the type, morphology and distribution of the precipitates containing Al and Si still need detailed analyses. In this work, the effects of alloying with the Al−Si eutectic alloy on the microstructure and mechanical properties of Mg−xLi (x=4, 8 and 12 wt.%) alloys were studied, and the aim was to focus on the strengthening effect and the mechanisms.

2 Experimental

Three alloys: Mg−4Li−3(Al−Si), Mg−8Li−3(Al−Si) and Mg−12Li−3(Al−Si) (wt.%) were prepared using magnetic-levitation, vacuum, high-frequency induction melting In this designation 3(Al−Si) represents 3 wt.% of the Al−12.6Si eutectic alloy. Appropriate quantities of pure Mg (99.95 wt.%), pure Li (99.95 wt.%) and the Al−12.6Si (wt.%) eutectic alloy were melted under an argon atmosphere. The melt was rapidly cooled by suction casting into a copper mold to form a cast rod with a dimension of d30 mm × 60 mm. The chemical compositions of the actual alloys are given in Table 1, which were detected by a plasma-atomic emission spectrometer (ICP-AES). The rod was cut into round plates: d30 mm × 10 mm. The plates were heated at 300 °C for 1 h and were then multi-pass rolled to a final thickness of 1.6 mm, with a reduction of about 20% for each pass, with an intermediate anneal at 300 °C for 15 min. The d130 mm-diameter rolls were preheated and maintained at 150 °C throughout the rolling. The rolled sheets were finally annealed at 150 °C for 1 h.

Table 1 Chemical compositions of actual alloys (wt.%)

Alloy	Li	Al	Si	Mg
Mg−4Li−3(Al−Si)	3.85	3.31	0.47	Bal.
Mg−8Li−3(Al−Si)	7.92	3.28	0.42	Bal.
Mg−12Li−3(Al−Si)	11.76	3.42	0.39	Bal.

Tensile specimens were prepared with a gauge length of 25 mm, a width of 5.7 mm and a thickness of 1.5 mm, according to the ASTM standards E8/E8M−2011. The tensile tests were performed on a CMT5205 electronic universal testing machine with a 0.5 mm/min tensile speed. The microstructure was examined using a scanning electron microscope (SEM, MIRA3) equipped with an Oxford electron backscattered diffraction (EBSD) system and energy dispersive spectroscopy (EDS), and a transmission electron microscope (TEM, JEOL−2100F). The samples for TEM examination were prepared by twin-jet electropolishing using a solution of 5% perchloric acid in ethanol at about −20 °C, and finally ion-milling for 30 min on a Gatan PIPS II machine.

3 Results and discussion

3.1 Microstructure

Figure 1 presents the grain orientation and (0002) pole figure of the annealed Mg−4Li−3(Al−Si) alloy. The EBSD data were cleaned up based on grain dilation type, whose grain tolerance angle was 5° and the minimum grain size was 4 μm. There were a few large grains whose size was about 15 μm, and small grains were distributed around the large grains. The highest texture intensity for the annealed Mg−4Li−3(Al−Si) alloy was 14.23. According to ZHAO et al [18], the precipitate phase particles in the Mg−4Li−3(Al−Si) alloy were

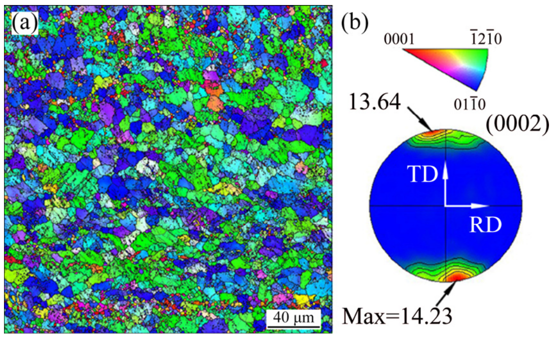

Fig. 1 Grain orientation image (a) and (0002) pole figure (b) of annealed Mg−4Li−3(Al−Si) alloy

Mg_2Si and Al_3Li. After rolling, there was no basal texture, indicating that the fine dispersed precipitates produced by Al−Si effectively inhibited the activation of basal slip.

Figure 2 shows EBSD data for the annealed Mg−4Li−3(Al−Si) alloy, which were used to analyze the grain boundary configuration and dynamic recrystallization. In Fig. 2(a), green represents low-angle grain boundaries (LAGB), and black represents high-angle grain boundary (HAGB). Figure 2(b) shows the distribution of grain size. The microstructure was mainly composed of LAGB, which was present in almost every large grain. This indicates that severe plastic deformation occurred during rolling, and a large number of dislocations accumulated in the grains and subgrain boundaries. Static recovery was predominant in the alloy during annealing, and there was not a high degree of recrystallization, which would lead to a dramatic reduction of dislocation density and grain refinement [19,20]. In Fig. 2(c), the red areas represent the deformed grains, the yellow areas represent the substructure, and the blue areas represent the recrystallized grains. The majority of grains were red deformed grains, and only a few recrystallized grains appeared at the junctions of tiny grains. Many factors can impact on dynamical recrystallization, in which precipitates could postpone or promote dynamical recrystallization, depending on the particle size, distribution and density of particles [18]. Obviously, the fine dispersed Mg_2Si and Al_3Li precipitates effectively pinned the grain boundaries of the α-Mg grains of the Mg−4Li−3(Al−Si) alloy during deformation and annealing, and restricted the grain recrystallization. In addition, the distribution of the yellow substructure was not uniform, which may be due to the uneven deformation during rolling. Figure 2(d) indicates that the red deformation grains had larger strains, while the yellow substructure had smaller strains. This shows that the substructure can relieve strain.

Figure 3 shows SEM images of the annealed Mg−4Li−3(Al−Si) alloy. Figure 3(a) shows coarse white laminar Mg_2Si elongated in the rolling direction. Higher magnifications (Figs. 3(b−d)) indicate tiny granular precipitates in addition to the white Mg_2Si. According to ZHAO et al [18], the second phase precipitates contained Al in the Mg−4Li−3(Al−Si) alloy are Al_3Li precipitates.

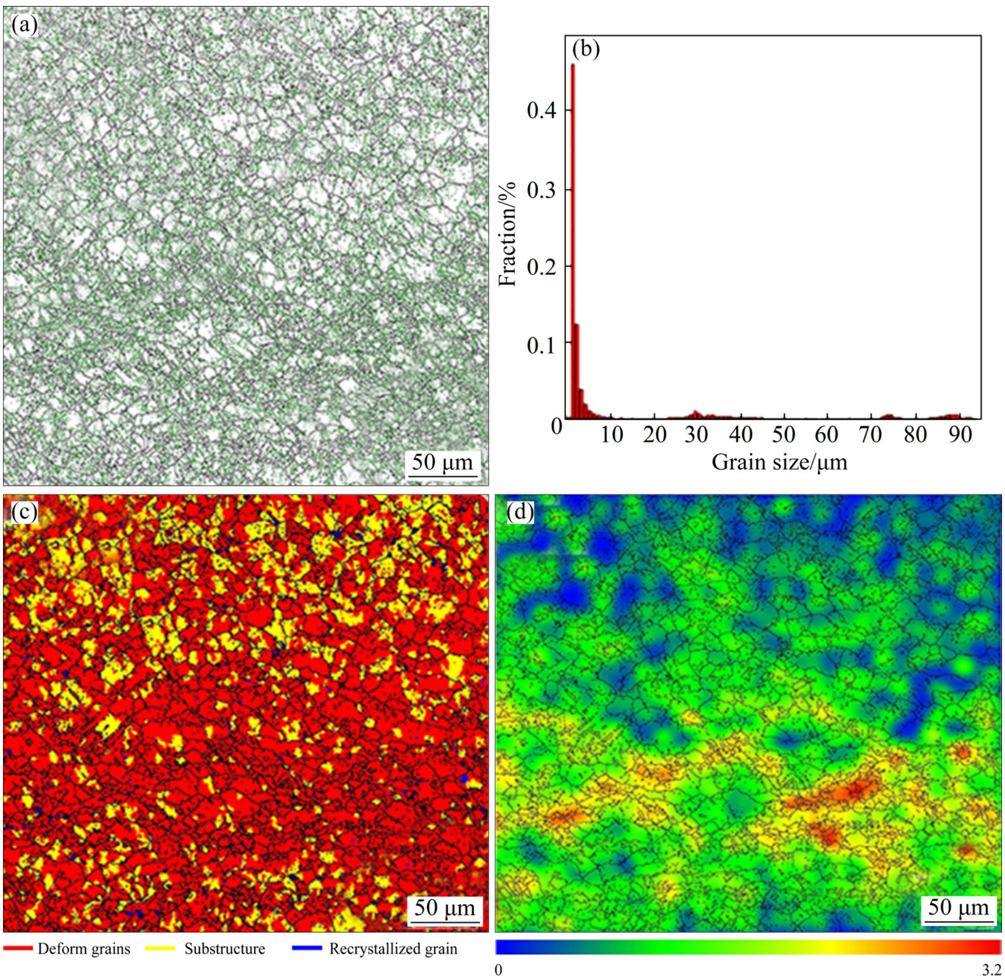

Fig. 2 Grain boundary and dynamic recrystallization of annealed Mg−4Li−3(Al−Si) alloy: (a) Grain boundary distribution; (b) Grain size distribution; (c) Dynamic recrystallization distribution; (d) Strain distribution

After rolling, the smaller particles were distributed in the microstructure uniformly, which enhanced the precipitation strengthening [21−23]. These results indicated that the strengthening mechanisms of the *α*-Mg in the Mg−4Li−3(Al−Si) alloy were solid solution hardening, precipitation hardening and strain hardening.

Figure 4 shows the SEM images and EDS mapping results of the annealed Mg−8Li−3(Al−Si) alloy Figure 4(a) indicates that the Mg−8Li−3(Al−Si) alloy consisted of strip-like α-phase and matrix β-phase. There were some small white granular precipitates existed on the surface. The distribution of Al was more uniform

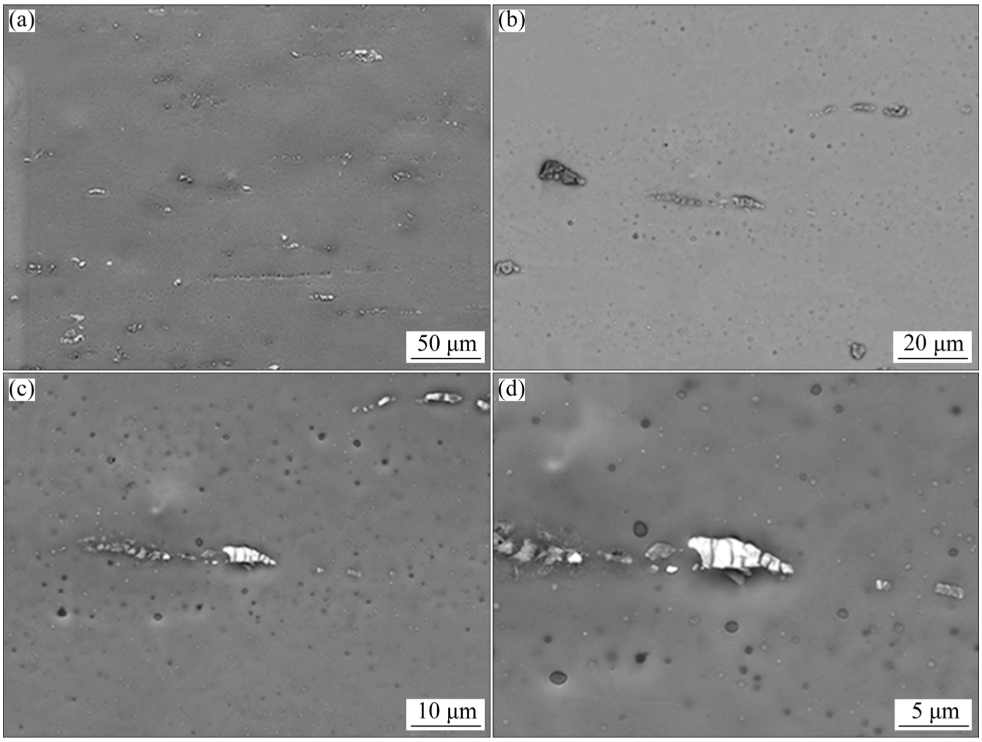

Fig. 3 SEM images of annealed Mg−4Li−3(Al−Si) alloy with different magnifications

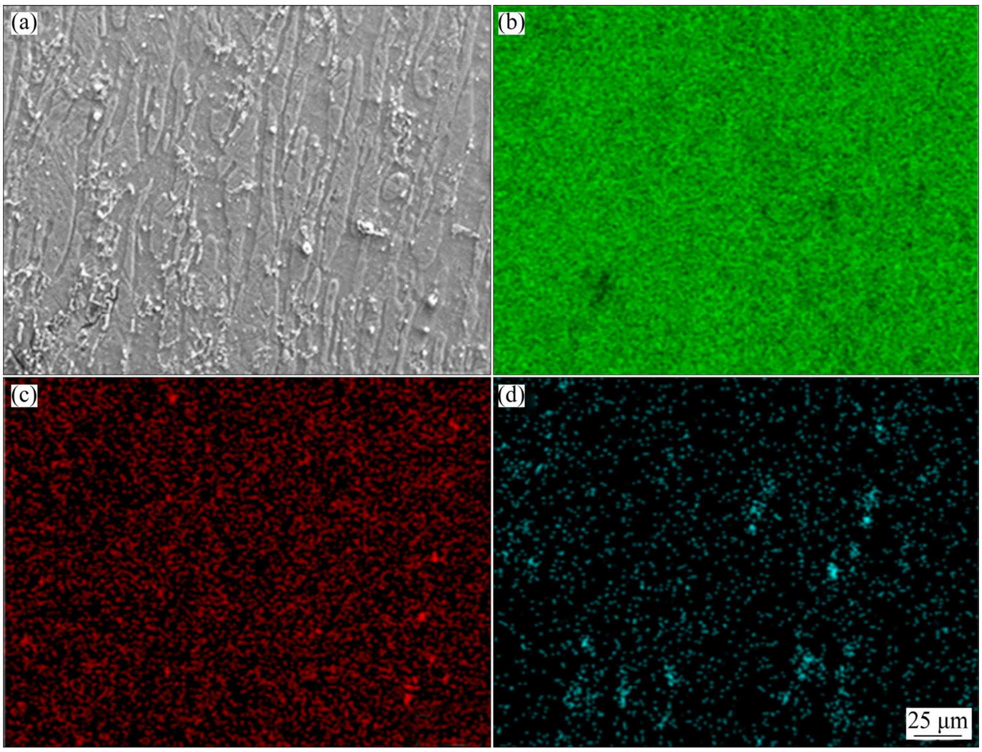

Fig. 4 SEM image (a) and EDS mapping scanning results (b, c, d) of annealed Mg−8Li−3(Al−Si) alloy: (a) SEM image; (b) Mg; (c) Al; (d) Si

(Fig. 4(c)) than Si, because Al element had a higher solid solubility in Mg, which showed solid solution strengthening effect in Mg matrix. Point-like segregations of Al and Si elements were distributed in the Mg alloys, indicating that there were second phase precipitates. According to Ref. [24], the distribution showed characteristics of Mg_2Si brittle precipitates, which was consistent with that observed in the Mg−4Li−3(Al−Si) alloy.

SEM images and EDS analysis results were taken to obtain more detailed information in the annealed Mg−8Li−3(Al−Si) alloy (Fig. 5). Figure 5(a) shows that the white acicular Mg_2Si particles were distributed along the α/β interface and mainly in the β-phase matrix which was attributed to the β-phase is the softer phase [25]. There was also a smaller gray particulate precipitate (Fig. 5(b)), which can be identified by EDS analysis. The precipitate contained only Al without Si, so the precipitate was AlLi phase according to Ref. [25]. ZHANG et al [26] reported that Mg alloys had poor corrosion resistance and were easy to oxidize. Thus, the oxygen content in Fig. 5 is attributed to the oxidation of the sample during processing.

Figure 6 presents SEM images of the annealed Mg−12Li−3(Al−Si) alloy. The microstructure was characterized by banded structure as shown in Fig. 6(a). Figures 6(b−d) show high-magnification images of fine particles which were uniformly dispersed in the β-Li matrix. The small white elongated particles were Mg_2Si phase precipitates and the grey granular particles were Al−Li phase precipitates, which were distributed along the rolling direction. These results show that the enhancement effect of Al−Si on α-phase might be different with that of β-phase, which is closely related to the crystal structure difference between α-Mg and β-Li.

To understand the interference with the matrix, a bare spherical precipitate in the annealed Mg−12Li−3(Al−Si) alloy was analyzed by TEM, as shown in Fig. 7. The EDS spectrum (Fig. 7(b)) and SAD pattern (Fig. 7(c)) were taken from the red-dash-circled area in Fig. 7(a). The EDS spectrum (Fig. 7(b)) shows mainly characteristic X-ray of Al, indicating that the spherical precipitate is the Al−Li phase. The SAED pattern (Fig. 7(c)) revealed that the spherical precipitate contains interplanar spacings of 0.232, 0.202, 0.141, 0.117 and 0.093 nm which matched the d-values of the planes $(01\bar{1}5)$, $(11\bar{2}3)$, $(02\bar{2}7)$, (0210) and $(04\bar{4}5)$ of Li_3Al_2, respectively. The error of interplanar spacings is minimal compared with the standard value. Thus, the spherical precipitate is the Li_3Al_2 phase.

3.2 Mechanical properties

The tensile stress−strain curves and histograms of mechanical properties of the annealed Mg−4Li−3(Al−Si), Mg−8Li−3(Al−Si) and Mg−12Li−3(Al−Si) alloys are shown in Figs. 8(a) and (b), respectively. The Mg−4Li−3(Al−Si) alloy exhibits the highest ultimate tensile strength (UTS) of 249 MPa but the lowest elongation of 6.3%. The Mg−12Li−3(Al−Si) alloy possesses the highest elongation of 26% but the lowest UTS of 173 MPa. The Mg−8Li−3(Al−Si) alloy has intermediate mechanical properties, with UTS of 210 MPa

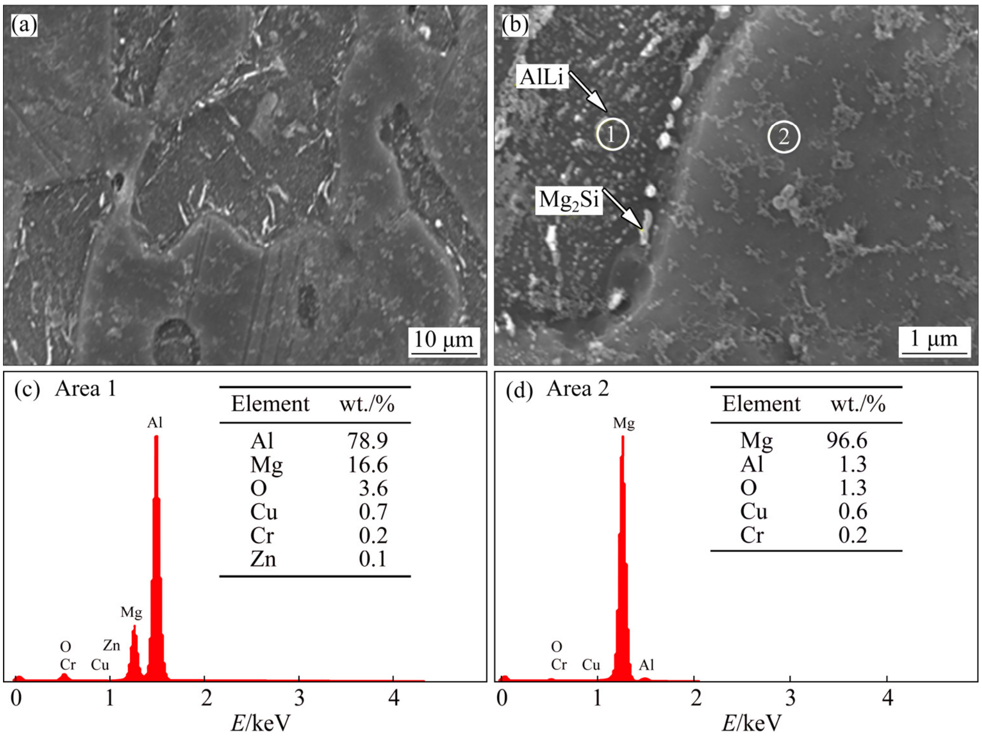

Fig. 5 High-magnification SEM images (a, b) and EDS analyses (c, d) of annealed Mg−8Li−3(Al−Si) alloy

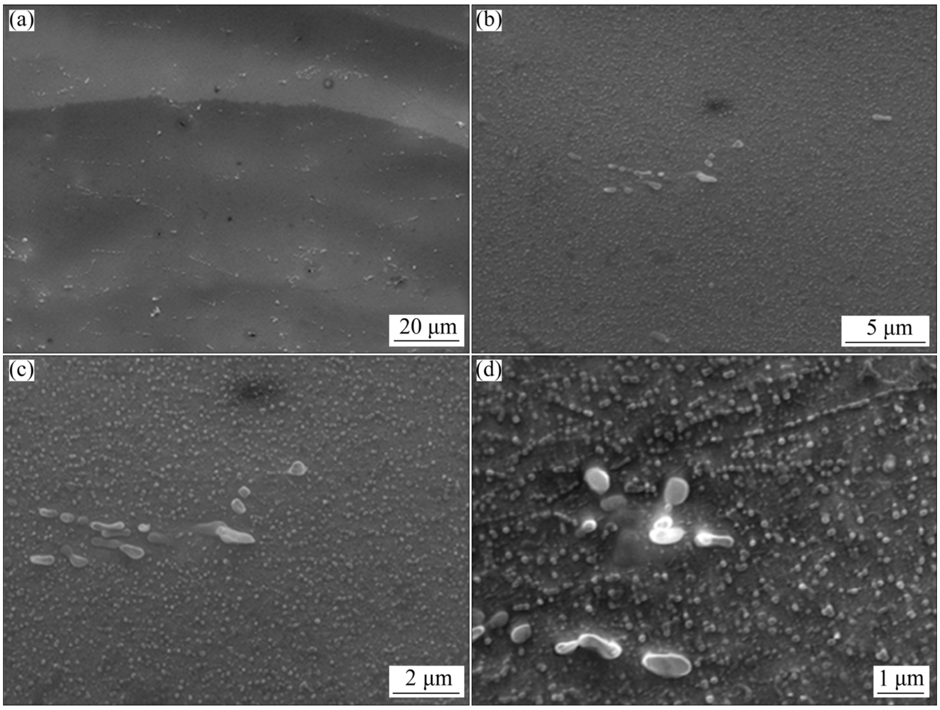

Fig. 6 SEM images of annealed Mg−12Li−3(Al−Si) alloy with different magnifications

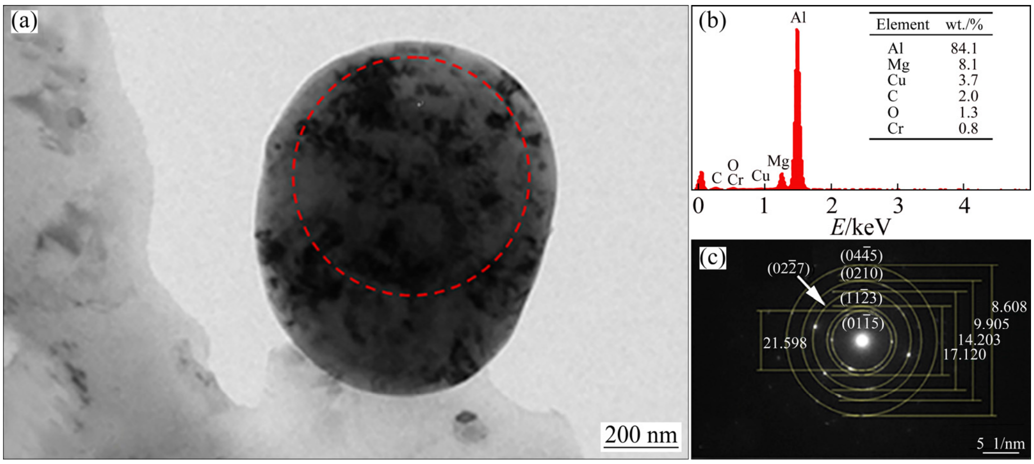

Fig. 7 TEM image (a) of precipitate in Mg−12Li−3(Al−Si) alloy, EDS spectrum (b) and SAD pattern (c) from red-dash-circled area in (a)

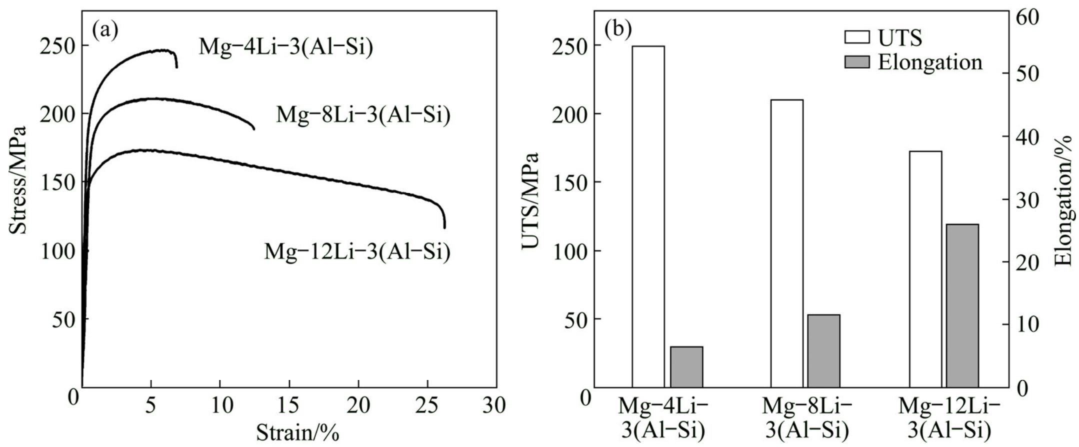

Fig. 8 Stress−strain curves and histograms of mechanical properties of as-rolled Mg−xLi−3(Al−Si) alloy

and an elongation of 11.6%. In comparison with the Refs. [27−29], the addition of Al−Si eutectic resulted in the increase of UTS but decrease of elongation of Mg−Li alloys. In addition, the results of tensile experiments indicate that the strengthening effect of Al−Si on the α-Mg based (Mg−4Li) is significantly higher than that of β-phase (Mg−12Li). The strength of the alloys decreased with the increase of Li content, while the elongation increased.

The reason why the three alloys show different tensile strength and elongation can be attributed to two affects. On one hand, the three alloys have three different phase structures, which are α-phase, (α+β)-phase and β-phase with increasing Li content. The α-phase possesses the HCP crystal structure and acts as a hard phase whilst the β-phase has the BCC crystal structure functioning as a soft phase [30,31]. On the other hand, the precipitates of the three alloys are different in composition and morphology. Besides Mg_2Si phase, the different precipitations of the Al−Li phases (including the Al_3Li, AlLi and Li_3Al_2 phase particles) were formed in the corresponding Mg−xLi (x=4, 8 and 12 wt.%) alloys. That is, the origin of the strengthening can be understood from the well-established theories of dislocation interactions in metals, which is usually a result of solid solution and precipitation effects, strain hardening, grain size reduction, or a combination of these effects [32]. Besides, crystal structure is closely related to the mechanical properties owing to soft β-phase [33−36].

4 Conclusions

(1) Alloying with the Al−Si eutectic causes different precipitates in the three alloys with α-phase, α+β dual-phase and β-phase. Besides Mg_2Si phase, the Al−Li phases of Mg−xLi−3(Al−Si) alloys (x=4, 8 and 12 wt.%) are Al_3Li, AlLi and Li_3Al_2 phase, respectively.

(2) The tensile strength of the Mg−xLi−3(Al−Si) alloys (x=4, 8 and 12 wt.%) decreases with increasing Li content, whilst the elongation increases. The Mg−4Li−3(Al−Si) alloy exhibits the highest UTS of 249 MPa and the Mg−12Li−3(Al−Si) alloy possesses the highest elongation of 26%.

(3) The strengthening effect of the Al−Si eutectic alloying on the α-phase (Mg−4Li) is higher than that on the β-phase (Mg−12Li), which might be related to the different crystal structures and the different category, morphology and distribution of the precipitate phases.

References

[1] ATRENS A, JOHNSTON S, SHI Zhi-ming, DARGUSCH M S. Viewpoint-understanding Mg corrosion in the body for biodegradable medical implants [J]. Scripta Materialia, 2018, 154: 92−100.

[2] LU Xiao-peng, BLAWERT C, TOLNAI D, SUBROTO T, KAINER K U, ZHANG Tao, WANG Fu-hui, ZHELUDKEVICH M L. 3D reconstruction of plasma electrolytic oxidation coatings on Mg alloy via synchrotron radiation tomography [J]. Corrosion Science, 2018, 139: 395−402.

[3] WANG Xian, LI Lin-xin, XIE Zhi-hui, YU Gang. Duplex coating combining layered double hydroxide and 8-quinolinol layers on Mg alloy for corrosion protection [J]. Electrochimica Acta, 2018, 283: 1845−1857.

[4] WU Liang, YANG Dan-ni, ZHANG Gen, ZHANG Zhi, ZHANG Sheng, TANG Ai-tao, PAN Fu-sheng. Fabrication and characterization of Mg−M layered double hydroxide films on anodized magnesium alloy AZ31 [J]. Applied Surface Science, 2018, 431: 177−186.

[5] ZHANG Gen, WU Liang, TANG Ai-tao, MA Yan-long, SONG Guang-ling, ZHENG Da-jiang, JIANG Bin, ATRENS A, PAN Fu-sheng. Active corrosion protection by a smart coating based on a MgAl-layered double hydroxide on a cerium-modified plasma electrolytic oxidation coating on Mg alloy AZ31 [J]. Corrosion Science, 2018, 139: 370−382.

[6] WU Yi-ping, XIONG Han-qing, JIA Yu-zhen, XIE Shao-hui, LI Guo-feng. Microstructure, texture and mechanical properties of Mg−8Gd−4Y−1Nd−0.5Zr alloy prepared by pre-deformation annealing, hot compression and ageing [J]. Transactions of Nonferrous Metals Society of China, 2019, 29: 976−983.

[7] MAHMUDI R, SHALBAFI M, KARAMI M, GERANMAYEH A. Effect of Li content on the indentation creep characteristics of cast Mg−Li−Zn alloys [J]. Materials & Design, 2015, 75: 184−190.

[8] ZENG Ying, JIANG Bin, LI Rui-hong, HE Jun-jie, XIA Xiang-sheng, PAN Fu-sheng. Effect of Li content on microstructure, texture and mechanical properties of cold rolled Mg−3Al−1Zn alloy [J]. Materials Science and Engineering A, 2015, 631: 189−195.

[9] LI C Q, XU D K, CHEN X B, WANG B J, WU R Z, HAN E H, BIRBILIS N. Composition and microstructure dependent corrosion behaviour of Mg−Li alloys [J]. Electrochimica Acta, 2018, 260: 55−64.

[10] TANG Yan, LE Qi-chi, MISRA R D K, SU Guan-qiao, CUI Jian-zhong. Influence of extruding temperature and heat treatment process on microstructure and mechanical properties of three structures containing Mg−Li alloy bars [J]. Materials Science and Engineering A, 2018, 712: 266−280.

[11] DONG Han-wu, WANG Li-min, LIU Ke, WANG Li-dong, JIANG Bin, PAN Fu-sheng. Microstructure and deformation behaviors of two Mg−Li dual-phase alloys with an increasing tensile speed [J]. Materials & Design, 2016, 90: 157−164.

[12] HOU Le-gan, WANG Tian-zi, WU Rui-zhi, ZHANG Jing-huai, ZHANG Mi-lin, DONG An-pin, SUN Bao-de, BETSOFEN S, KRIT B. Microstructure and mechanical properties of Mg−5Li−1Al sheets prepared by accumulative roll bonding [J]. Journal of Materials Science & Technology, 2018, 34: 317−323.

[13] CAO Fu-rong, ZHOU Bi-jin, DING Xin, ZHANG Jian, XU Guang-ming. Mechanical properties and microstructural evolution in a superlight Mg−7.28Li−2.19Al−0.091Y alloy fabricated by rolling [J]. Journal of Alloys and Compounds, 2018, 745: 436−445.

[14] FU Xue-song, YANG Yan, HU Jia-wei, SU Jun-fei, ZHANG Xue-ping, PENG Xiao-dong. Microstructure and mechanical properties of as-cast and extruded Mg−8Li−1Al−0.5 Sn alloy [J]. Materials Science and Engineering A, 2018, 709: 247−253.

[15] ZENG Ying, JIANG Bin, LI Rui-hong, YIN Heng-mei, AL-EZZI S. Grain refinement mechanism of the as-cast and as-extruded Mg−14Li alloys with Al or Sn addition [J]. Metals, 2017, 7: 172.

[16] LIU T, WU S D, Li S X, LI P J. Microstructure evolution of Mg−14%Li−1%Al alloy during the process of equal channel angular pressing [J]. Materials Science and Engineering A, 2007, 460: 499−503.

[17] SHI Quan-xin, BIAN Li-ping, LIANG Wei, CHEN Zhi-qiang, YANG Fu-qian, WANG Yi-de. Effects of adding Al−Si eutectic alloy and hot rolling on microstructures and mechanical behavior of Mg−8Li alloys [J]. Journal of Alloys and Compounds, 2015, 631: 129−132.

[18] ZHAO Zi-long, SUN Zi-wei, LIANG Wei, WANG Yi-de, BIAN Li-ping. Influence of Al and Si additions on the microstructure and mechanical properties of Mg−4Li alloys [J]. Materials Science and Engineering A, 2017, 702: 206−217.

[19] LEVINSON A, MISHRA R K, DOHERTY R D, KALIDINDI S R. Influence of deformation twinning on static annealing of AZ31 Mg alloy [J]. Acta Materialia, 2013, 61: 5966−5978.

[20] CHAO H Y, SUN H F, CHEN W Z, WANG E. Static recrystallization kinetics of a heavily cold drawn AZ31 magnesium alloy under annealing treatment [J]. Materials Characterization, 2011, 62: 312−320.

[21] LIU Huan, XUE Feng, BAI Jing, MA Ai-bin, JIANG Jing-hua. Formation behavior of 14H long period stacking ordered structure in Mg−Y−Zn cast alloys with different α-Mg fractions [J]. Journal of Materials Science & Technology, 2016, 32: 1267−1273.

[22] PARK G H, KIM J T, PARK H J, KIM Y S, JEONG H J, LEE N, SEO Y, SUH J Y, SON H T, WANG W M, PARK J M, KIM K B. Development of lightweight MgLiAl alloys with high specific strength [J]. Journal of Alloys and Compounds, 2016, 680: 116−120.

[23] WEI Guo-bing, MAHMOODKHANI Y, PENG Xiao-dong, HADADZADEH A, XU Tian-cai, LIU Jun-wei, XIE Wei-dong, WELLS M A. Microstructure evolution and simulation study of a duplex Mg−Li alloy during double change channel angular pressing [J]. Materials & Design, 2016, 90: 266−275.

[24] LU L, CHEN X, HUANG X, LU K. Revealing the maximum strength in nanotwinned copper [J]. Science, 2009, 323: 607−610.

[25] ZHAO Zi-long, XING Xue-gang, LUO Yi, LIANG Wei. Influence of Al−Si additions on mechanical properties and corrosion resistance of Mg−8Li dual-phase alloys [J]. Journal of Iron and Steel Research International, 2017, 24: 426−429.

[26] ZHANG Gen, WU Liang, TANG Ai-tao, ZHANG Shuo, YUAN Bo, ZHENG Zhi-cheng, PAN Fu-sheng. A novel approach to fabricate protective layered double hydroxide films on the surface of anodized Mg−Al alloy [J]. Advanced Materials Interfaces, 2017, 4: 1700163.

[27] LI C Q, XU D K, YU S, SHENG L Y, HAN E H. Effect of icosahedral phase on crystallographic texture and mechanical anisotropy of Mg−4%Li based alloys [J]. Journal of Materials Science & Technology, 2017, 33: 475−480.

[28] ZHANG M L, WU R Z, WANG T. Microstructure and mechanical properties of Mg−8Li−(0−3)Ce alloys [J]. Journal of Materials Science, 2009, 44: 1237−1240.

[29] YAN Hong, CHEN Rong-shi, HAN En-hou. Microstructures and mechanical properties of cold rolled Mg−8Li and Mg−8Li−2Al−2RE alloys [J]. Transactions of Nonferrous Metals Society of China, 2010, 20(S): s550−s554.

[30] WU Rui-zhi, QU Zhi-kun, ZHANG Mi-lin. Effects of the addition of Y in Mg−8Li−(1, 3) Al alloy [J]. Materials Science and Engineering A, 2009, 516: 96−99.

[31] WANG Tao, ZHANG Mi-lin, WU Rui-zhi. Microstructure and properties of Mg−8Li−1Al−1Ce alloy [J]. Materials Letters, 2008, 62: 1846−1848.

[32] XU Wan-qiang, BIRBILIS N, SHA Gang, WANG Yu, DANIELS J E, XIAO Yang, FERRY M. A high-specific-strength and corrosion-resistant magnesium alloy [J]. Nature Materials, 2015,14: 1229−1235.

[33] LI Qiang, QIU Yue-xiu, LI Bo, ZHAO Dong-liang, SUN De-en, LI De-hui. Silicon strengthened CrAlVN coatings [J]. Journal of Iron and Steel Research International, 2015, 22: 1118−1125.

[34] CAO Lei, YANG Zhong-min, CHEN Ying, WANG Hui-min, ZHAO Xiao-li. Effects of nitrogen content and austenitization temperature on precipitation in niobium micro-alloyed steels [J]. Journal of Iron and Steel Research International, 2015, 22: 1164−1173.

[35] XU D K, WANG B J, LI C Q, ZU T T, HAN E H. Effect of icosahedral phase on the thermal stability and ageing response of a duplex structured Mg−Li alloy [J]. Materials & Design, 2015, 69: 124−129.

[36] XU D K, LI CQ, WANG B J, HAN E H. Effect of icosahedral phase on the crystallographic texture and mechanical anisotropy of duplex structured Mg−Li alloys [J]. Materials & Design, 2015, 88: 88−97.

Li 含量对 Mg−*x*Li−3(Al−Si)合金显微组织和力学性能的影响

张 诚[1,2]，吴 量[1,2]，赵子龙[3]，谢治辉[4]，黄光胜[1,2,5]，刘 磊[1,2]，蒋 斌[1,2,5]，Andrej ATRENS[6]，潘复生[1,2,5]

1. 重庆大学 材料科学与工程学院，机械传动国家重点实验室，重庆 400044；
2. 重庆大学 国家镁合金材料工程技术研究中心，重庆 400044；3. 重庆大学 土木工程学院，重庆 400045；
4. 西华师范大学 化学化工学院 化学合成与污染控制四川省重点实验室，南充 637002；
5. 重庆市科学技术研究院 重庆市先进材料研究中心，重庆 401123；
6. School of Mechanical and Mining Engineering, The University of Queensland, Brisbane Qld 4072, Australia

摘 要：基于 α-Mg、α-Mg+β-Li 和 β-Li 三种相结构，制备 Mg−4Li−3(Al−Si)、Mg−8Li−3(Al−Si)和 Mg−12Li−3(Al−Si)三种合金，用于研究 Al−Si 共晶体对其组织和力学性能的影响。在 Mg−*x*Li (x=4%, 8%和 12%，质量分数)合金中添加 Al−Si 共晶体分别形成以下的 Al−Li 析出相：Al_3Li、AlLi 和 Li_3Al_2。此外，在这三种合金中还发现大量的 Mg_2Si 相颗粒。拉伸试验结果表明，Mg−4Li−3(Al−Si)合金的极限抗拉强度最高，为 249 MPa，其伸长率最低，为 6.3%。Mg−12Li−3(Al−Si)合金的伸长率最高，为 26%，但极限抗拉强度最低，为 173 MPa。这三种合金力学性能的差异归因于晶体结构的不同以及析出物类型、形态和分布的不同。

关键词：Mg−Li 合金；Al−Si 共晶体；第二相；抗拉强度；伸长率

(Edited by Xiang-qun LI)